24th COBEM - 2017

24th ABCM International Congress of Mechanical Engineering
December 3-8, 2017, Curitiba, PR, Brazil

COBEM-2017-2080
BALL ON PLANE ROLLING TESTS TO EVALUATE GEARS CONTACT FATIGUE

Pedro Del Negro Tayer
Newton K Fukumasu
Rodrigo Lima Stoeterau
Izabel Fernanda Machado
Universidade de São Paulo, PMR-EP-USP, Av. Prof. Mello Moraes, 2231, 05508930, São Paulo, Brazil.
pedro.negro.tayer@gmail.com
fukumasu@gmail.com
rodrigo.stoeterau@usp.br
machadoi@usp.br

Guilherme Antonio Assis Machado
Fiat Chrysler Automobiles (FCA), Av. Contorno, 3455, 32669-900, Minas Gerais, Brazil.
guilherme.antonio@fcagroup.com

Abstract. *One of the possible mechanisms of gear failure can be related to the cyclic loading and, as a consequence, the fatigue occurrence. The onset of fatigue failure occurs due to stress intensifiers and it is generally observed on the fillet (bending fatigue) or on the flank contact region (contact fatigue). Gear fatigue evaluation is usually carried out by test rigs, which are expensive. An alternative method of contact fatigue test of gears is evaluated in this work, which consists of balls rolling on a plane (specimen). Two groups of specimens were manufactured to obtain microstructural features and mechanical properties similar to gears tooth's surface: a) with shot-peening and b) without shot-peening. The different features of specimens were tested by using an in house developed equipment to evaluate the rolling contact fatigue (RCF), which occurs on gears on its diametral pitch. Results indicate the occurrence of two failure modes: pitting and spalling. Also, the shot-peened group specimens presented lower fatigue life resistance for the analyzed conditions, which are not in agreement with the literature. This discrepancy may be related to the elevated contact pressure applied to accelerate the tests (3 GPa), which may promote a deeper subsurface damage, disregarding the protective effect shot-peening generated at the surface of the samples.*

Keywords*: gears, rolling contact fatigue, shot-peening, spalling, pitting.*

1. INTRODUCTION

In April 2012, the Brazilian government announced the creation of a new national automotive polity. Called *INOVAR AUTO*, it aims to increase the competitiveness, technology and safety of cars produced and sold in Brazil through investment in research and development (R & D), innovation, local engineering, basic industrial technology, suppliers capacity, national content and energy efficiency between 2012 and 2017 (Ferreira Filho et al., 2013).

The *INOVAR AUTO* program encourages the relationship between universities and automakers. Within this concept, the *PROGRAMA DE RESIDÊNCIA TECNOLÓGICA PARA ENGENHEIROS* (Technological Residency Program for Engineers) was created, with the objective of researching and stimulating innovation through a partnership with scholarship students, master's level, with exclusive dedication to the theme, to work with engineering professionals in the development of research on themes in the Fiat Chrysler Automobiles (FCA) portfolio of current projects (De Souza, Bracarense and Massarani, 2016). The automotive transmission system is one of the mechanical components whose program aims to improve, being composed of several components, such as bearings, shafts and gears.

The most common mode of gear failure is surface contact fatigue (Fernandes and McDuling, 1997; Ding and Rieger, 2003). Contact fatigue broadly refers to the surface damage process, such as pitting, wear debris formation and fatigue cracking, induced by cyclic contact between two surfaces. (Suresh, 1998).

Fatigue tests of gears are usually conducted through test rigs, which are expensive, mainly due to instrumentation and high dimensional precision required for the specimens. Moreover, different damage mechanisms occur along this

kind of experiments so that, at the end of the test, the surface usually presents characteristics that can difficult the analysis of each damage mechanism in particular.

Therefore, an attempt to evaluate gear fatigue was conducted in this work. The pure rolling phenomenon that occurs on the diametral pitch of a gear was reproduced by means of bearing balls rolling on a plane, by using in-house developed equipment (Neves, 2006). Figure 1a presents the relative velocity between two teeth surfaces along the contact region (Suresh, 1998). In this figure, the sliding velocity is null at pitch line, meaning that only rolling is present. In this way, the ball on disk test may be able to recover the type of damage that occurs on tooth pitch line (Figure 1b).

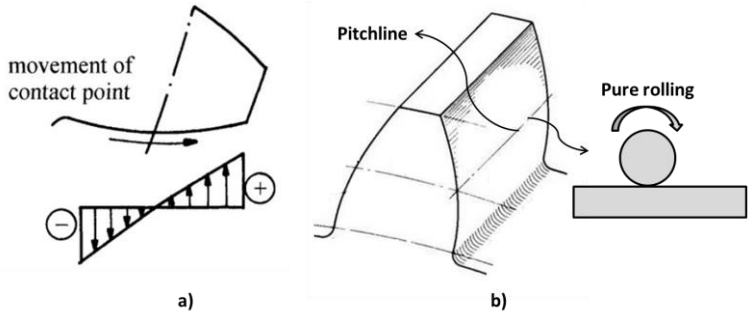

Figure 1. a) Relative surface velocity among the contact point of a gear tooth; b) Proposed system modeling

In this work, pure rolling condition is obtained by rolling ball on a disk test configuration, allowing the analyses of different types of surface damage found in the primitive diameter of gears (pitchline) subjected to contact fatigue. Also, the influence of surface properties, induced by shot-peening process, on rolling contact fatigue (RCF) life is evaluated.

2. EXPERIMENTAL PROCEDURE

In order to obtain surface damage found in the pitch line of gears, both load and lubricant temperature are controlled during the rolling ball on disk test, in which surface integrity of the disk is evaluated. Tests are run on a built in-house equipment (Neves, 2006), used to characterize RCF failure modes. Surface damage produced by the tests was analyzed to evaluate the surface topography of the disk using an optical interferometry technique before and after tests.

2.1 Materials

Specimens used in this work were made of ABNT 4320 steel, which is a chrome-nickel-molybdenum alloy widely used to manufacture gears, shafts and pinions. The nominal chemical composition is presented in Tab. 1.

Table 1. Nominal chemical composition of steel ABNT/AISI 4320 (ArcelorMittal, 2013).

Element	Carbon	Manganese	Phosphor	Sulfur	Silicon	Nickel	Chrome	Molybdenum
Composition (%)	0.17 - 0.22	0.45 - 0.65	≤ 0.030	≤ 0.040	0.15 - 0.35	1.65 - 2.00	0.40 - 0.60	0.20 - 0.30

All the specimens were grounded to improve surface finishing and avoid geometrical errors. Further, the samples were submitted to a carbonitriding process to increase surface hardness. The specimen main features and dimensions are shown on Fig. 2.

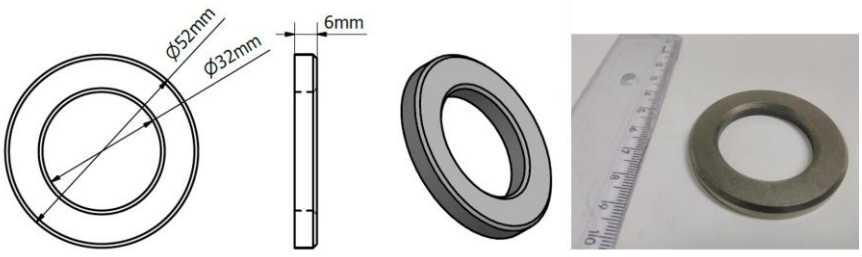

Figure 2. Specimens' dimensions

In order to evaluate the influence of shot-peening on RCF life, the specimens were separated into different groups: without shot-peening (group N) and with shot-peening (group S). The shot-peening process was performed to improve the surface integrity of about 50 μm below the grounded surface.

The spheres (counter bodies) were made of ABNT 52100 steel, which is a chrome alloy used to make rolling bearing spheres. The spheres have a nominal diameter of 7.938 mm (5/16") and hardness of about 890 HV. The nominal chemical composition is presented in Tab. 2.

Table 2. Nominal chemical composition of steel ABNT52100 (ArcelorMittal, 2013).

Element	Carbon	Manganese	Phosphor	Sulfur	Silicon	Nickel	Chrome	Molybdenum
Composition (%)	0.98 - 1.10	0.25 - 0.45	≤ 0.025	≤ 0.025	0.15 - 0.35	-	1.30 - 1.60	-

2.2 Specimens Characterization

Surface roughness, topography and damage features were analyzed by optical interferometry in Taylor Hobson CCI MP equipment. Measurements were performed in about 15 different regions on each specimen. Each region measurement corresponded to an area of 2.9 mm². The roughness cut-off parameters were selected following ISO 4288.

Roughness measurements were carried out in 5 different regions inside the wear track, after the rolling ball on disk tests to evaluate the variation on roughness due to wear. These measurements were conducted on 3 specimens of N and S groups.

Vickers hardness of the surface was performed using 20 kgf load. A total of 5 measurements of each specimen were carried out in different regions of the surface. The hardness was also measured at the transversal section (hardness along the specimen depth) using a Hysitron TI950 triboindenter and the results obtained in previous work of Fukumasu (2016) are also present to improve the discussion. The Oliver and Phaar method was used to calculate the hardness based on the indentation load curves.

2.2.1 Damage Characterization

Optical interferometry analysis of the worn surface was performed to characterize the failure mechanisms on all specimens. It is worth mentioning that there are two most dominant mechanisms for RCF, i.e., the subsurface originated spalling and surface originated pitting (Sadeghi et al., 2009) and no unified definitions have been established in the literature to consistently distinguish pitting from spalling; one of the reasons for the confusion is probably due to the fact that the physical causes of pitting and spalling have not yet been established (Ding and Rieger, 2003; Santus et al., 2012).

Nevertheless, there is a tendency to define pitting as damage initiated at the surface caused by surface defects and asperities and generate shallow craters (depths lower than 10 μm). The pitting occurrence is expected when the specific film thickness (Λ) is lower than 1 and it is mostly caused by asperities or surface defects contact (Santus et al., 2012). The spalling is related to subsurface initiated damage that generate deeper cavities with the depth near the region of the maximum Hertz orthogonal shear stress (OSS) (Ding and Rieger, 2003; Sadeghi et al., 2009; Santus et al., 2012). Also, pitting occurs for higher values of Rq and spalling predominates on other cases, and the pitting usually occurs before spalling (Piao et al., 2012). According to this classification, spalling and pitting are not different stages of the same phenomenon but different damage mechanisms, distinguished by the position where the crack initiates (Santus et al., 2012). Hence, in this work, analysis of damage depth generated on the worn surface was carried out to characterize the failure mechanism.

2.3 Experiments

2.3.1 Equipment

The machine used in this work was projected and built in house (Neves, 2006) to analyze contact fatigue of rollers. In this system, an accelerometer is responsible to detect the material failure at ball on disk contact region due to a subtle increase in vibration of the system.

Load is applied by a lever arm using dead weights. The load alignment is maintained using a spherical coupling between the chamber and the lever. Figure 3 displays a section view of the equipment's chamber, in which the contact occurs. The chamber is filled with lubricant whose temperature is monitored by a thermocouple, allowing temperature control near the contact region. An external pump provides temperature controlled water to maintain the temperature of the chamber.

Figure 4 shows a picture of the system and the positions of the accelerometer, the thermocouple and the load application support.

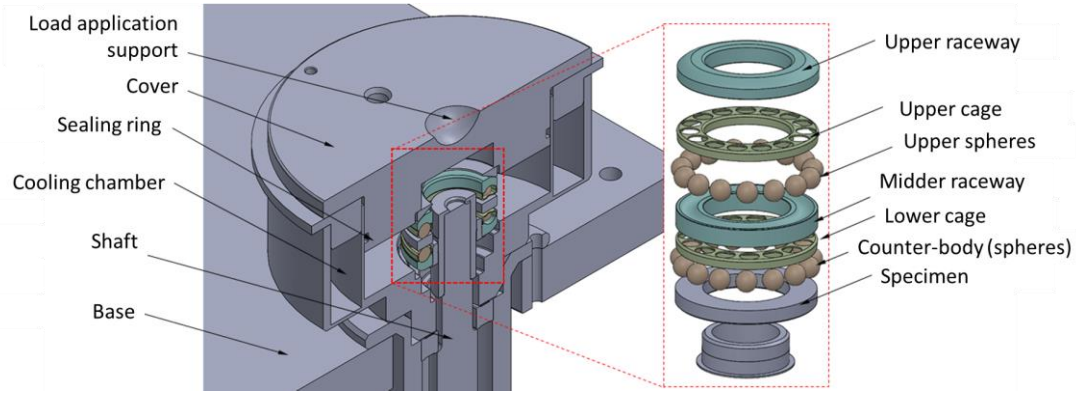

Figure 3. Section view of RCF machine chamber

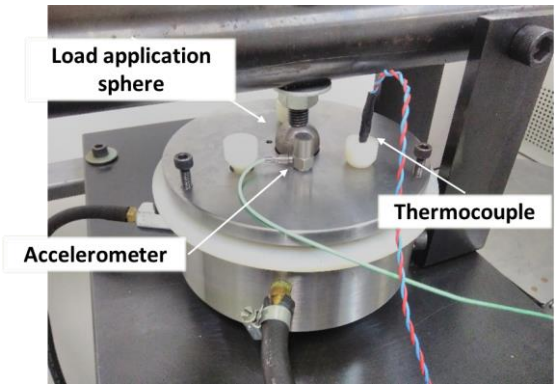

Figure 4. Photograph of RCF machine chamber's cover

2.3.2 Analyzed parameters

Automotive gears present specific conditions on the pitch line during the gear coupling that can be reproduced by the RCF system. However, the tribological tests would take long runs to present similar surface damages found in gears. Therefore, in this work, several parameters were tested to achieve the optimized set that may cause surface damage in accelerated tests. Hence, the contact pressure was set at 3 GPa, which is about 1.5 times higher than the regular contact pressures presented during the gear coupling. Due to equipment limitations, the entrainment speed in the contacting region of the RCF machine was set at 3.86 m/s, which is lower than the entrainment velocity of automotive gears on the pitch line and it could affect the lubrication conditions.

The lubricant used in the tests was a commercial automotive transmission oil, composed of a synthetic base oil designated API GL4 with viscosity index SAE 75W. The temperature of the oil was maintained constant at 45±5 °C at the oil reservoir.

A total of 8 test replications was carried for each test group. Table 3 summarizes the experimental parameters

Table 3. Experimental parameters

Specimen material	AISI 4320 carbonitrided
Specimen surface treatment (2)	Unpeened (N) ; Shot-peened (S)
Sphere material	AISI 52100
Lubricant	GL4, SAE 75W
Maximum contact pressure	3 GPa
Lubricant temperature	45±5 °C
Entrainment Velocity	3.86 m/s

2.4 Statistical Analyses

The two-parameter Weibull distribution is used in this work to model durability predictions (time-to-fail) of the surface, in which a goodness-of-fit test, based on a graph method, was carried on for the failure times obtained by the increase on the system vibration (Tiryakioglu and Hudak, 2011).

The maximum likelihood estimation (MLE) method was conducted to find the two Weibull parameters that can best fit the obtained data. The confidence bounds were calculated with 90% confidence level.

3. RESULTS AND DISCUSSION

3.1 Hardness of the samples

Vickers hardness measurements are displayed in Figure 6. These results indicate a slight increase on surface hardness of group S, and it can be related to the shot-peening process. The maximum indentation depth was about 20 μm, which is in the region affected by the shot-peening.

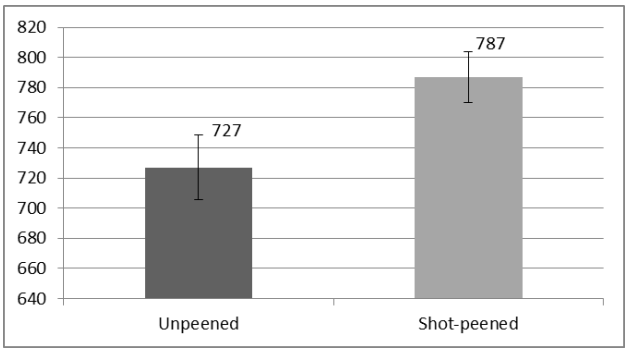

Figure 6. Surfaces hardness for both groups of specimens

The hardness along the depth on the transversal section of the specimen for both groups is presented in Figure 7a. The shot-peening process didn't appear to cause significant difference at the near surface region. Fukumasu et al. (2016) measured hardness with the same method for deeper regions on a similar material without shot-peening (Figure 7b). This figure indicates a decreasing hardness profile associated to the carbonitrided layer, which ranges from top surface down to 0.8 mm.

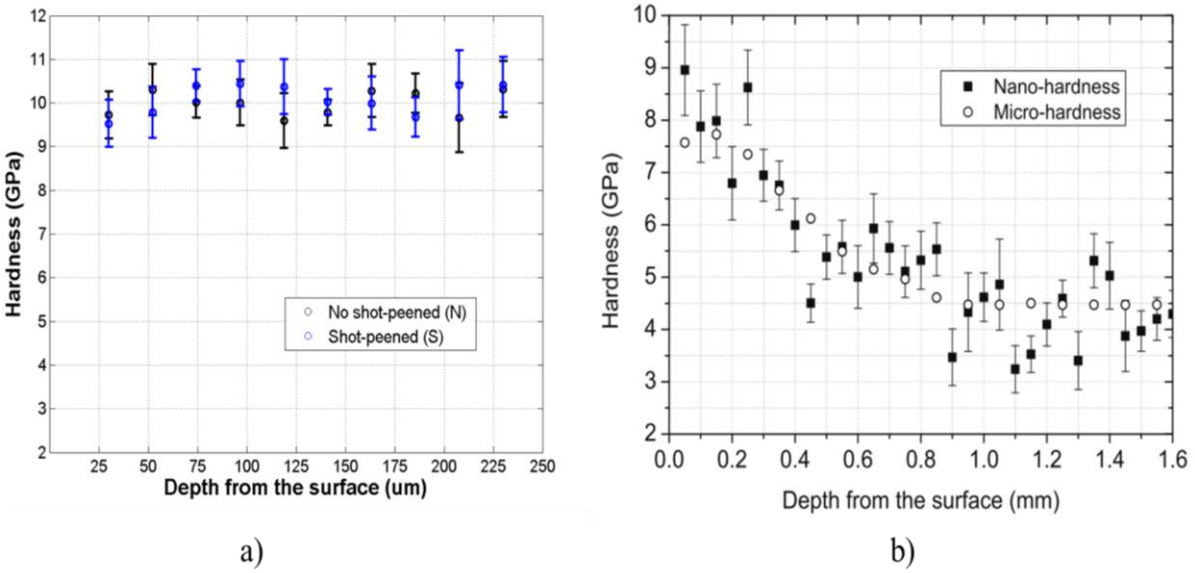

Figure 7. Hardness measurements along the depth in a transversal section: a) nanoindentation hardness profile measurement done in this work and b) nanoindentation hardness profile measured by Fukumasu et al. (2016).

3.2 Roughness and specific film thickness

Surface topography and roughness parameters (ISO25178) for the surfaces with and without shot-peening are shown in Table 4. Both surfaces present similar topography features regarding the roughness parameters, nevertheless some spatial differences on asperity distribution can be observed.

Significant reduction on Sq values ranging from 54% to 67% was obtained after the tests inside the wear track. This is an indicative of surface wear, in which roughness parameters are changing throughout the tests. It is worth noting the contact between asperities on the surfaces was expected concerning low values of oil specific film thickness calculation (Λ) based on Stachowiak and Batchelor (1993) work. Λ is shown in Table 5. The low values of specific film thickness indicate a boundary or mixed lubrication condition, in which asperities may become in contact during the tests.

The lesser reduction of Sq after test and the boundary lubrication condition at the contact region of the specimen with shot-peening (group S) may indicate a reduction on the surface wear given by the higher surface hardness and due the residual stresses generated by the shot-peening process. Focusing on the Sq roughness parameter, Figure 5 indicates the comparison between the measurements before and after the RCF experiments.

Table 4. Roughness parameters values for both groups of specimens (N and S groups)

Group analyzed	Sq (μm)	Ssk	Sku	Sk (μm)	Spk (μm)	Svk (μm)
Unpeened - N 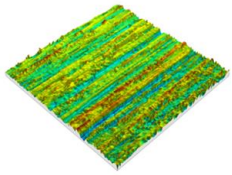	1.04 ± 0.20	-0.51 ± 0.51	4.19 ± 1.09	0.99 ± 0.08	0.42 ± 0.08	0.61 ± 0.10
Shot-peened - S 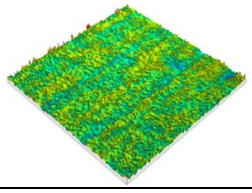	1.16 ± 0.21	-0.56 ± 0.41	4.19 ± 1.11	0.89 ± 0.05	0.39 ± 0.04	0.55 ± 0.07

Table 5. Specific film thickness (Λ) for both groups of specimens, before and after the experiments. N_B: unpeened before test; S_B: shot-peened before test; N_A: unpeened after test; and S_A: shot-peened after test

	S_B	N_B	S_A	N_A
Λ	0.09	0.08	0.29	0.19

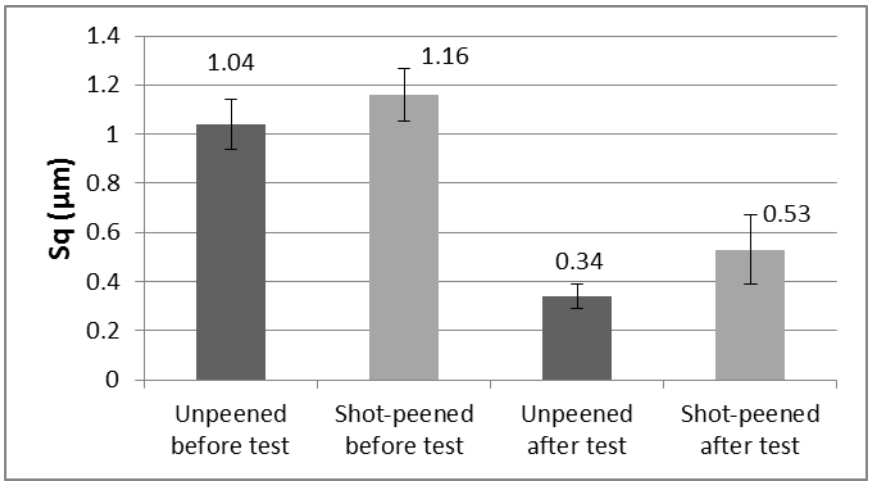

Figure 5. Roughness values for both groups of specimens, before and after experiments.

3.3 Damages produced at the wear track

In the present work, the pitting was generated on both tested groups (with and without shot-peening). A shallow damage located at the same depth scale as the roughness was found, as shown generally on Fig. 8a, which represents a pitting damage at the race track of group N specimen. This figure indicates craters formed with about 4 µm in depth for both groups N and S.

However, it is worth mentioning that pitting did not cause a subtle raise on vibration signal and, consequently, this is the reason the occurrence of these kind of damage was not instantly detected.

On the other hand, the spalling occurrence increased vibration signal. This kind of damage was observed in all specimens, forming a punctual crater with a depth associated to the Hertz maximum orthogonal shear stress depth, as shown in Fig. 8b. This figure shows the race track of a group S representative specimen, in which the damage occurred at a maximum depth of 53 µm from the surface.

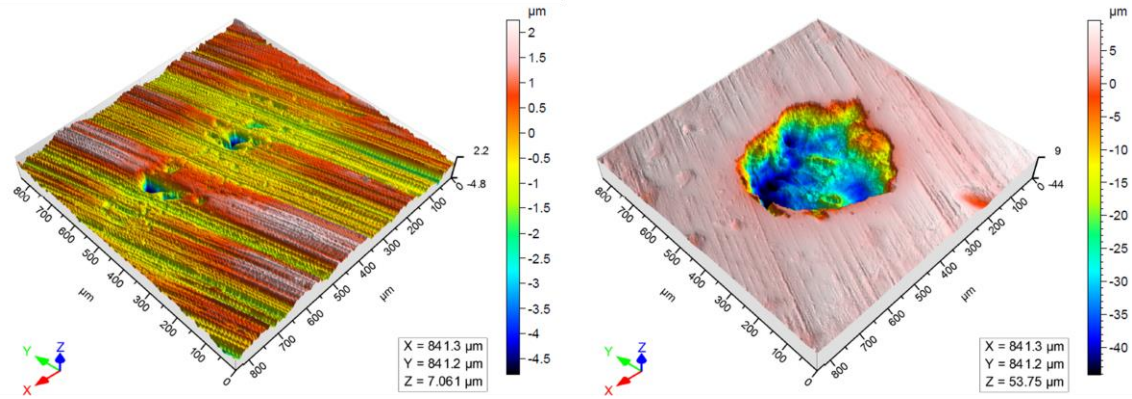

a) b)

Figure 8. a) Pitting surface generated (N group); b) Spalling subsurface generated (S group)

Table 4 indicates the values of stresses parameters occurring at the contact region. In this table, both maximum Hertz pressure and maximum shear stress were calculated following Johnson et al. (1985), while maximum orthogonal shear stress and its depth were calculated based on Hamrock and Dowson (1981) and Moyar and Sharma (1997). These are important parameters to characterize the surface failure mechanism.

Table 4. Main stress parameters of the experiments

Load per sphere	177 N
Maximum Hertz Contact Pressure	3.0 GPa
Maximum shear stress ($\tau_{máx}$)	930.3 MPa
Depth of maximum shear stress ($Z\tau_{máx}$)	80.5 µm
Maximum orthogonal shear stress ($\tau_{xymáx}$)	641.9 MPa
Depth of maximum orthogonal shear stress ($Z\tau_{xymáx}$)	58.9 µm

The spalling depths of all specimens were measured and the average results and standard deviation are shown in Fig. 9. It is important to point out the proximity of Hertz maximum orthogonal shear stress depth ($Z\tau_{xymáx}$ = 58.9 µm) in the N group and the proximity of the theoretical limit of shot-peening's affected layer (LSPL = 50 µm) in the S group. These results indicate that the critical depth for the N group is associated to the maximum orthogonal shear stress depth, while for the S group, the critical depth would be the interface between shot-peening affected layer and bulk material. The interface region is critical since it denotes an important gradient in stresses, going from high compressive values (shot-peened region) to low values (non-affected region).

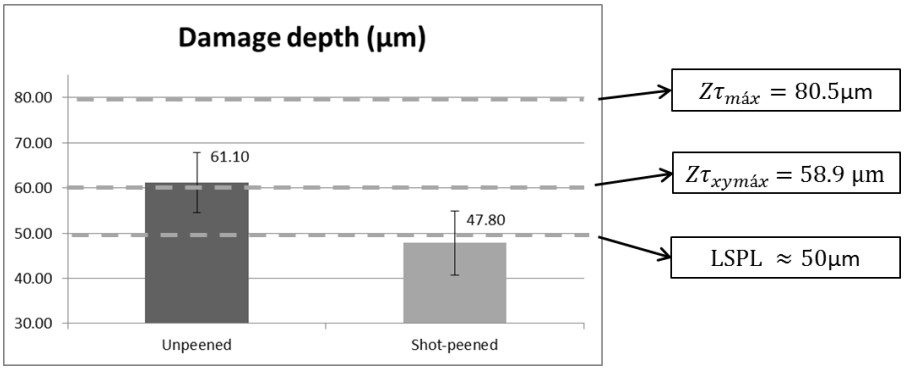

Figure 9. Average damage depths for both groups of specimens. $Z\tau_{máx}$: depth of maximum shear stress (80.5 µm); $Z\tau_{xymáx}$: depth of maximum orthogonal shear stress (58.9 µm); LSPL: theoretical limit of shot-peened layer (50 µm).

3.4 Fatigue life

Figure 10 presents the Weibull cumulative fail probability plots for both groups S and N. The bounds represent 90% confidence level calculated by MLE. The failure, as mentioned before, is considered as the raise on vibration signal, probably due to spalling generation. From this figure, the shot-peening group presents lower life compared to the group without shot-peening.

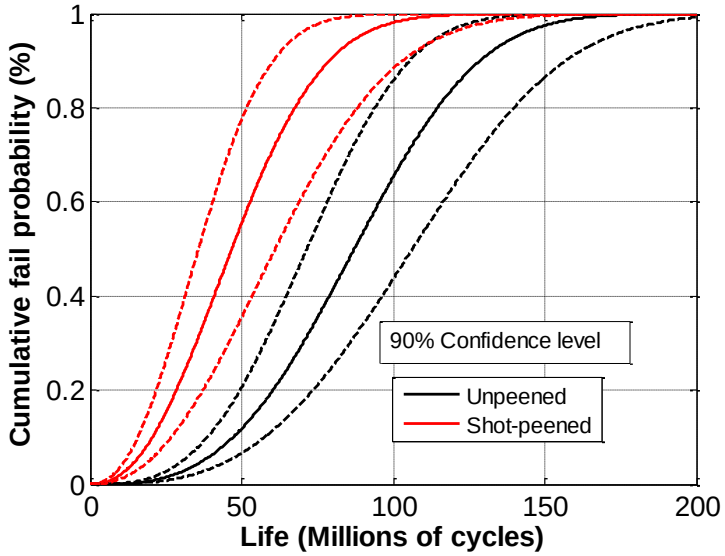

Figure 10. Cumulative fail probability Weibull plot for both groups of specimens

The lower time-to-failure of the group S RCF tests, although contradictory, may have some substantial explanations whose are further discussed.

There are many important potential pitfalls that could cause an accelerated life test to lead to incorrect conclusions. Appropriate use of accelerated test methods requires careful consideration of the underlying failure mechanisms and the effect of accelerating variables may have on these mechanisms (Meeker and Escobar, 1998).

Firstly, in this work, the shot-peening process was similar to a commercial process used in the automotive gears industry. It was set to produce a compressive residual stressed layer of about 50 µm in thickness, considering the gear regular stress conditions. The RCF tests imposed a Hertz maximum contact pressure of 1.5 times higher than regular contact pressures presented during the gear coupling. Consequently, the stress distribution changed and was moved towards a deeper position. One can assume that the shot-peening affected layer, adjusted to the regular gear scenario, may not be deep enough to present similar effect on the RCF critical depths. The orthogonal shear stresses as a function of depth calculated based on Moyar and Sharma (1997) and using 2 and 3 GPa maximum Hertz pressure conditions (regular gear coupling and RCF present work experiments, respectively) are shown on Fig. 11.

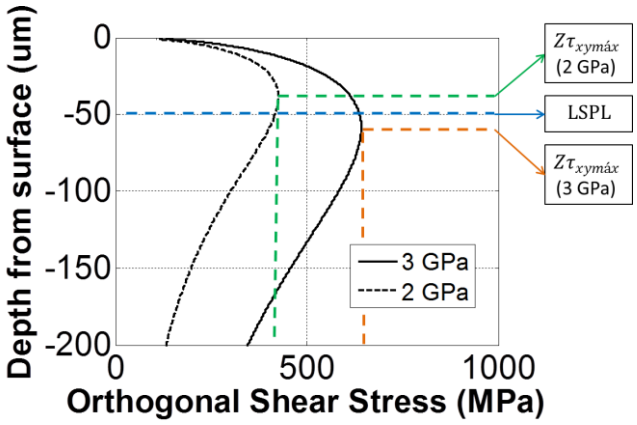

Figure 11. Orthogonal shear stress along depth. $Z\tau_{xymáx}(2\ GPa)$: depth of maximum orthogonal shear stress for 2 GPa maximum Hertz pressure (40.0 μm); $Z\tau_{xymáx}(3\ GPa)$: depth of maximum orthogonal shear stress for 3 GPa maximum Hertz pressure (58.9 μm); LSPL: theoretical limit of shot-peened layer (50 μm).

Hence, for the regular gear coupling condition at 2 GPa maximum Hertz pressure, the critical depth, $Z\tau_{xymáx}\ (2\ GPa)$ is located inside the shot-peening affected layer. On the other hand, for 3 GPa maximum Hertz pressure RCF set in the present work, the critical depth, $Z\tau_{xymáx}\ (3\ GPa)$ is located outside the shot-peening affected layer, which indicates the benefits of shot-peening are not achieved because the thickness of shot-peening affected layer is shallower than the critical depth for the accelerated RCF experiments. Furthermore, the interface of the shot-peening layer behaves as a stress raiser, promoting crack nucleation and propagation in this region. This result is corroborated by the average spalling depth, which correlates directly to the position of this interface on RCF accelerated tests.

4. CONCLUSIONS

The ball on plane pure rolling tests reproduced the damages found in the primitive diameter of gears denominated as pitting and spalling. However, it appears to be capable of detecting just the occurrence of spalling. The occurrence of pitting seems not promote a significant rise on vibration signal.

The rolling contact fatigue critical depth was detected at the spalling depth. The depth where spalling cracks nucleate was different for each group, since the limit of shot-peening layer appears to behave like a stress raiser and it promoted the crack nucleation on the interface of the shot-peening region. Then, this interface depth was the critical depth for shot-peened specimen while the maximum orthogonal shear stress depth was the critical depth for unpeened specimens.

The shot-peening process resulted in the worst rolling contact fatigue life in this work, mainly due to the elevated contact pressure applied to accelerate the tests (3 GPa), which promoted a deeper subsurface damage, disregarding the protective effect of the shot peening generated at the surface of the samples.

5. ACKNOWLEDGEMENTS

The authors would like to thank Fiat Chrysler Automobiles - FCA for their financial support and to encourage automotive technological development in Brazil through the PROGRAMA INOVAR FCA – UNIVERSIDADES - RESIDÊNCIA TECNOLÓGICA PARA ENGENHEIROS. The authors also would like to thank FAPESP, CNPq and CAPES.

6. REFERENCES

ArcelorMittal, 2013, "Guia do Aço", 15 May 2017. < http://Brazil.arcelormittal.com.br/pdf/quem-somos/guia-aco.pdf>.

de Souza, G. L., Bracarense, A. Q. and Massarani, M. “Residência Tecnológica para Engenheiros.” I*n Simpósio Internacional de Engenharia Automotiva - SIMEA 2016*. São Paulo, Brazil, 2016.

Ding, Y. and Rieger, N. F., 2003, "Spalling formation mechanism for gears", *Wear*, Vol. 254, pp. 1307-1317.

Fernandes, P., McDuling, C., 1997, "Surface contact fatigue in gears", *Engineering Failure Analysis*, Vol. 4, pp. 99-107.

Ferreira Filho, V. S., et al., 2013, “Inovar-Auto & Alianças Estratégicas: Um novo cenário de cooperação para Montadoras e Fornecedores de Autopeças.”. In *X SEGet–Simpósio de Excelência em Gestão e Tecnologia*. Porto Alegre, Brazil.

Fukumasu, N. K., Machado, G. A. A., Souza, R. M. and Machado I. F., 2016, "Stress Analysis to Improve Pitting Resistance in Gear Teeth". *Procedia CIRP*, Vol. 45, pp. 255-258.

Hamrock, B. J. and Dowson, D., 1981, "Ball Bearing Mechanics". NASA Technical Memorandum 81691.

Johnson, K. L., 1985, "Contact Mechanics", Cambridge University Press, Cambridge, England, 452 p.

Liu, W., Dong, J., Zhang, P., Zhai, C. and Ding, W., 2009, "Effect of Shot Peening on Surface Characteristics and Fatigue Properties of T5-Treated ZK60 Alloy". *Materials Transactions*, Vol. 50, pp. 791-798.

Meeker, W. Q. and Escobar, L. A., 1998, "Pitfalls of Accelerated Testing". *IEEE Transactions on Reliability*, Vol. 47, pp. 114-118.

Moyar, G. J. and Sharma V., 1997, "Orthogonal Shear Stress Amplitude as a Function of Rolling Contact Ellipticity and Depth". Journal of Tribology, Vol. 199, pp 883-886.

Neves, J. C. K., 2006, "Desenvolvimento de um equipamento para ensaio de fadiga de contato esfera sobre plano e sua aplicação na caracterização de ferros fundidos com matrizes de elevada dureza" PhD Thesis, Universidade de São Paulo, São Paulo.

Piao, Z., Xu, B., Wang, H. and Wen, D., 2012, "Influence of Surface Roughness on Rolling Contact Fatigue Behavior of Fe-Cr Alloy Coatings". *Journal of Materials Engineering and Performance*, Vol. 22, pp. 767-773.

Sadeghi, F., Jalalahmadi, B., Slack, T. S. and Raje, N., 2009, "A review of Rolling Contact Fatigue", Journal of Tribology, Vol. 131, p. 041403-12.

Santus, C., Beghini, M., Bartilotta, I. and Facchini, M., 2012, "Surface and subsurface rolling contact fatigue characteristic depths and proposal of stress indexes", International Journal of Fatigue, Vol. 45, pp. 71-81.

Suresh, S., 1998, "Fatigue of Materials", Cambridge University Press, Cambridge, England, 679 p.

Tiryakioglu, M. and Hudak, D., 2011, "Guidelines for two-parameter Weibull analysis for flaw-containing materials". *Metallurgical and Materials Transactions B: Process Metallurgy and Materials Processing Science*, Vol.42, pp. 1130-1135.

7. RESPONSIBILITY NOTICE

The authors are the only responsible for the printed material included in this paper.